Genomic DNA damage and ATR-Chk1 signaling determine oncolytic adenoviral efficacy in human ovarian cancer cells

Claire M. Connell,[1,2] Atsushi Shibata,[2] Laura A. Tookman,[1] Kyra M. Archibald,[1] Magdalena B. Flak,[1] Katrina J. Pirlo,[1] Michelle Lockley,[1] Sally P. Wheatley,[2] and Iain A. McNeish[1]

[1]Centre for Molecular Oncology and Imaging, Barts Cancer Institute, Queen Mary University of London, London, United Kingdom.
[2]Genome Damage and Stability Centre, University of Sussex, Brighton, United Kingdom.

Oncolytic adenoviruses replicate selectively within and lyse malignant cells. As such, they are being developed as anticancer therapeutics. However, the sensitivity of ovarian cancers to adenovirus cytotoxicity varies greatly, even in cells of similar infectivity. Using both the adenovirus E1A-CR2 deletion mutant *dl*922-947 and WT adenovirus serotype 5 in a panel of human ovarian cancer cell lines that cover a 3-log range of sensitivity, we observed profound overreplication of genomic DNA only in highly sensitive cell lines. This was associated with the presence of extensive genomic DNA damage. Inhibition of ataxia telangiectasia and Rad3-related checkpoint kinase 1 (ATR-Chk1), but not ataxia telangiectasia mutated (ATM), promoted genomic DNA damage and overreplication in resistant and partially sensitive cells. This was accompanied by increased adenovirus cytotoxicity both in vitro and in vivo in tumor-bearing mice. We also demonstrated that Cdc25A was upregulated in highly sensitive ovarian cancer cell lines after adenovirus infection and was stabilized after loss of Chk1 activity. Knockdown of Cdc25A inhibited virus-induced DNA damage in highly sensitive cells and blocked the effects of Chk1 inhibition in resistant cells. Finally, inhibition of Chk1 decreased homologous recombination repair of virus-induced genomic DNA double-strand breaks. Thus, virus-induced host cell DNA damage signaling and repair are key determinants of oncolytic adenoviral activity, and promoting unscheduled DNA synthesis and/or impeding homologous recombination repair could potentiate the effects of oncolytic adenoviruses in the treatment of ovarian cancer.

Introduction

Oncolytic viruses multiply selectively within infected cancer cells and cause death, with the release of mature viruses that infect neighboring cells. The adenovirus deletion mutant *dl*922-947 contains a 24-bp deletion (amino acids 122–129) in the E1A-CR2 region, which binds to E2F-pRb complexes, thereby dissociating E2F to drive cells into an S phase–like state, allowing transactivation of genes necessary for viral DNA replication (1). We have previously shown that *dl*922-947 has considerable activity in ovarian cancer and is more potent than E1A WT adenoviruses and the E1B-55K mutant *dl*1520 (Onyx-015, H101) (2, 3). *dl*922-947 replicates selectively in cells with abnormalities of the Rb pathway and consequent G_1/S checkpoint, defects seen in over 90% of human cancers (4). Multiple different Rb pathway abnormalities have been described in ovarian cancer (5, 6), and, even in ovarian cancer cells that are readily infected with adenovirus serotype 5 (Ad5) vectors, there is huge variability in sensitivity to *dl*922-947–mediated cell death. In addition, the mechanisms by which oncolytic adenoviruses induce cell death in cancer cells remain unclear (7).

We recently showed that early expression of E1A correlated well with cell sensitivity to *dl*922-947 (8). Upon infection, E1A is the first adenoviral protein to be expressed and is required for the efficient transcription of other viral early genes (9) as well as the disruption of pRb-E2F complexes (1). We have previously shown that *dl*922-947 activity is also associated with deregulation of multiple cell cycle checkpoints, which accelerates cell cycle progression and enhances efficacy (10).

However, one consequence of such deregulated cell cycle progression is unscheduled replication of cellular DNA, which will activate the DNA damage signaling pathways whose function is to preserve the integrity of the cellular genome (11). Two key kinases are central to DNA damage responses, ataxia telangiectasia mutated (ATM) and ataxia telangiectasia and Rad3-related (ATR). ATM is classically activated by double-strand breaks (DSBs), whereas ATR can be activated by a wide variety of DNA events, including replication-associated DNA damage, resected DSB ends, and nucleotide excision repair. When activated, both trigger a series of signaling events and activate downstream cellular proteins, such as the checkpoint kinases 1 and 2 (Chk1 and Chk2). Both ATM and ATR can be activated by adenovirus infection (12, 13). However, the virus can evade some DNA damage responses: for example, E4orf3 causes immobilization of the MRN complex, which can inhibit ATR signaling (14), while MRE11 is degraded in response to the activity of the E1B55K/E4orf6 complex (15), which blocks signaling downstream of ATM. Nonetheless, infected cells still demonstrate some evidence of DNA damage signaling in the form of H2AX phosphorylation (13, 16).

We sought to explore the link between genomic DNA replication, DNA damage responses, and the overall efficacy of oncolytic adenoviruses in ovarian cancer. Our findings suggest that host cell DNA damage responses induced by aberrant genomic DNA replication strongly influence the potency of adenoviruses. Highly sensitive cells displayed profound overreplication of genomic DNA with

Authorship note: Claire M. Connell and Atsushi Shibata contributed equally to this work.

Conflict of interest: The authors have declared that no conflict of interest exists.

Citation for this article: *J Clin Invest* doi:10.1172/JCI43976.

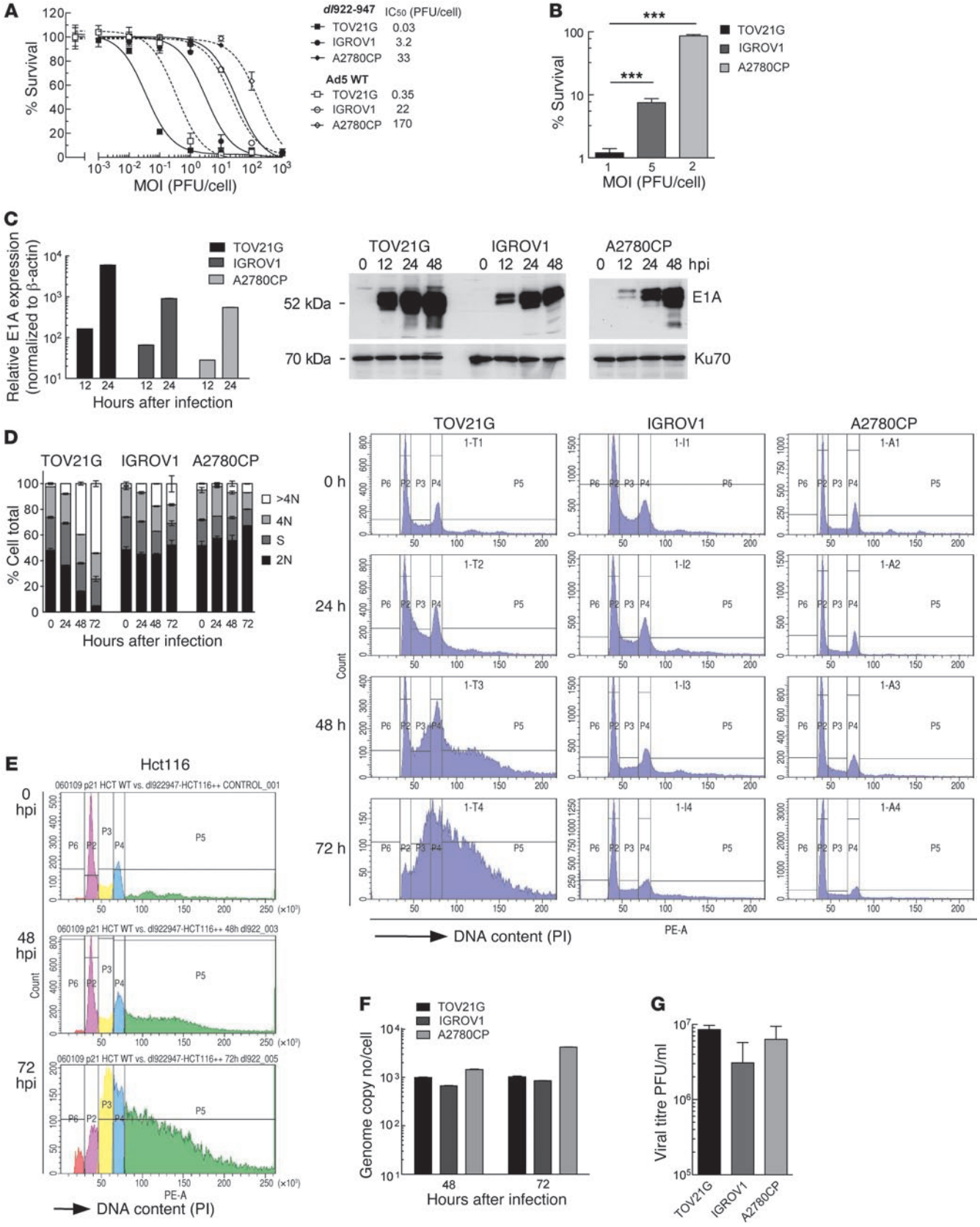
A
% Survival
MOI (PFU/cell)
dl922-947 IC50 (PFU/cell)
TOV21G 0.03
IGROV1 3.2
A2780CP 33
Ad5 WT
TOV21G 0.35
IGROV1 22
A2780CP 170
B
% Survival
MOI (PFU/cell)
TOV21G
IGROV1
A2780CP
***
C
Relative E1A expression (normalized to β-actin)
Hours after infection
TOV21G
IGROV1
A2780CP
0 12 24 48 hpi
52 kDa
70 kDa
E1A
Ku70
D
% Cell total
Hours after infection
>4N
4N
S
2N
0 h
24 h
48 h
72 h
Count
DNA content (PI)
PE-A
E
Hct116
0 hpi
48 hpi
72 hpi
DNA content (PI)
F
Genome copy no/cell
Hours after infection
G
Viral titre PFU/ml

Figure 1
Positive correlation between virus sensitivity and overreplication phenotype after *dl*922-947 infection in ovarian cancer cell lines. (**A**) Cell survival in TOV21G, IGROV1, and A2780CP cells was assessed by MTT assay 120 hpi with *dl*922-947 and Ad5 WT. (**B**) Survival of TOV21G, IGROV1, and A2780CP cells 120 hpi with *dl*922-947 at MOIs that permit 50% cell infectivity (MOI 1, 5, and 2 PFU/cell, respectively; data not shown). ***$P < 0.001$. (**C**) Expression of E1A was assessed by quantitative RT-PCR and immunoblot after infection with *dl*922-947 (MOI 7.5). Transcription is normalized to β-actin and presented relative to that of uninfected cells. Error bars (representing SD) are plotted on all data points but may be too small to be visible. (**D**) TOV21G, IGROV1, and A2780CP cells were harvested up to 72 hpi with *dl*922-947 (MOI 7.5), fixed in 70% cold ethanol, stained with PI, and analyzed by flow cytometry. >4N, cells with more than 4 N DNA content; 4N, cells with 4 N DNA content; S, cells in S phase; 2N, cells with 2 N DNA content. (**E**) Hct116 cells were harvested up to 72 hpi with *dl*922-947 (MOI 7.5), fixed in 70% cold ethanol, stained with PI, and analyzed by flow cytometry. IC_{50} for Hct116 cells 120 hpi with *dl*922-947 is approximately 0.04 PFU/cell (data not shown). (**F** and **G**) Replication of *dl*922-947 was assessed in TOV21G, IGROV1, and A2780CP cells after infection with *dl*922-947 (MOI 7.5) by quantitative PCR (**E**) 48 and 72 hpi and (**F**) by $TCID_{50}$ 72 hpi.

associated DNA damage and downstream signaling after infection with *dl*922-947. Moreover, inhibition of the ATR-Chk1 pathway increased genomic DNA overreplication and damage by preventing Chk1-mediated degradation of the Cdc25A phosphatase. Furthermore, Chk1 inhibition increased the number of DSBs, the most cytotoxic form of DNA damage, by preventing homologous recombination (HR) and increased sensitivity to *dl*922-947 activity both in vitro and in vivo. Similar results were observed after WT adenovirus infection, demonstrating that our findings are not specific to E1A-CR2 deletion mutants. Importantly, inhibition of the ATR-Chk1 pathway augmented sensitivity to adenovirus in cancer cells without affecting nonmalignant cells. As clinical trials of E1A-CR2–deleted adenoviruses have commenced (17), a better understanding of cellular responses to virus infection is vital and would open up the prospect of increased anticancer activity in patients.

Results

Adenovirus-induced cytotoxicity is associated with overreplication of cellular DNA in sensitive cells. The sensitivity of cancer cell lines to the oncolytic adenovirus *dl*922-947 varies considerably, even in cells with similar infectivity (8). TOV21G, IGROV1, and A2780CP are 3 ovarian cancer cell lines that cover a range of sensitivities, with IC_{50} values varying over 3 log scales (Figure 1A). The same wide range of sensitivity was seen with E1A WT adenoviruses (Figure 1A and Supplemental Figure 1A; supplemental material available online with this article; doi:10.1172/JCI43976DS1), although the WT viruses were consistently less potent in cancer cells than *dl*922-947, as seen before (3). The wide variation of sensitivity was not caused by differences in infectivity, as there were profound differences in cell survival at MOI that permitted 50% cells to be infected (Figure 1B). *E1A* is the first adenovirus gene to be expressed (18). As before, we found that early E1A transcription and protein expression correlated with cellular sensitivity to adenovirus (Figure 1C).

Cell cycle analysis revealed a stark contrast between the profiles of sensitive and insensitive cells after infection. TOV21G cells readily accumulated DNA contents of more than 4 N after *dl*922-947 infection; by 72 hours, the proportion of TOV21G cells with a DNA content of more than 4 N exceeded 50%. In IGROV1 cells, of intermediate sensitivity, the proportion reached 16.3% but only reached 7.0% in insensitive A2780CP cells, with little change throughout the course of infection (Figure 1D). Analysis of Hct116, another highly sensitive cancer line (*dl*922-947 $IC_{50} \approx$ 0.04 PFU/cell; data not shown), yielded similar cell cycle profiles to those of TOV21G cells, with a DNA content of more than 4 N of 58% by 72 hours after infection (hpi) (Figure 1E), while another resistant line, SKOV3ip1, generated profiles very similar to those of A2780CP cells (data not shown). Ad5 WT infection caused overreplication in TOV21G cells, although the proportion of cells with more than 4 N DNA was lower, reaching 34% 72 hpi (Supplemental Figure 1B). Thus, the effects seen with *dl*922-947 are not unique to ovarian cancer cells or to E1A-CR2 adenoviral deletion mutants, but they are greater than those seen with WT virus. The quantity of viral DNA generated in A2780CP cells was at least as great as that in the more sensitive TOV21G and IGROV1 cell lines (Figure 1F), indicating that the overreplication phenotype does not represent viral DNA but is a consequence of cellular DNA replication, consistent with previous reports (19, 20). In addition, the differential sensitivity amongst the cell lines was uncoupled from infectious virion production, with no significant difference in the number of virions produced in the 3 cell lines (Figure 1G). Adenovirus-induced cytotoxicity therefore appears not to depend upon the extent of virion production.

Oncolytic adenovirus cytotoxicity is associated extensive genomic DNA damage. Aberrant initiation of cellular DNA replication induces the accumulation of replication-associated DNA lesions (11, 21). To assess the extent of such DNA damage, cells were harvested up to 72 hpi with *dl*922-947, and phosphorylation of H2AX (ser 139; γH2AX) was analyzed immunocytochemically by flow cytometry with propidium iodide (PI) counterstaining to define cell cycle phase (22). Mock-infected cells displayed little γH2AX. In contrast, a huge increase in γH2AX was detectable in sensitive TOV21G cells after infection, and this increase occurred specifically in S and G_2/M cells and cells with more than 4 N DNA content (Figure 2A), indicating that DNA damage occurred after replication; at 48 hpi, over 90% of the overreplicated cells were γH2AX positive, compared with less than 10% γH2AX positivity in the G_1 population. Even in the insensitive A2780CP cells, in which there was minimal overreplication, the large majority of γH2AX positivity was seen in the S, G_2/M, and more than 4 N DNA content populations; by 48 hpi, only 7.9% cells were overreplicated, but 83% of these were γH2AX positive, whereas 60% of cells remained in G_1 phase, of which only 1% were γH2AX positive (Figure 2A).

It is known that expression of E1A can induce chromosomal aberrations (23). To assess the relationship between E1A expression and γH2AX, cells were infected with *dl*922-947 or a nonreplicating E1-deleted Ad5 vector, and the intensity of γH2AX and E1A within individual cells was assessed by immunofluorescence (IF) intensity over 48 hours (Figure 2, B and C). Infection with the nonreplicating vector induced no increase in γH2AX (data not shown). After *dl*922-947 infection, E1A and γH2AX increased in both sensitive and insensitive cell lines over time, and there was a strong positive correlation between the 2 across both cell lines ($r^2 = 0.879$, Pearson $r = 0.937$, $P = 0.0006$; Supplemental Figure 2A). However, the increases in both E1A and γH2AX were significantly greater in TOV21G cells than in A2780CP cells (Figure 2C and Supplemental Figure 2B). In addition, we identified a positive correlation between γH2AX and BrdU signals ($r^2 = 0.692$, Pearson

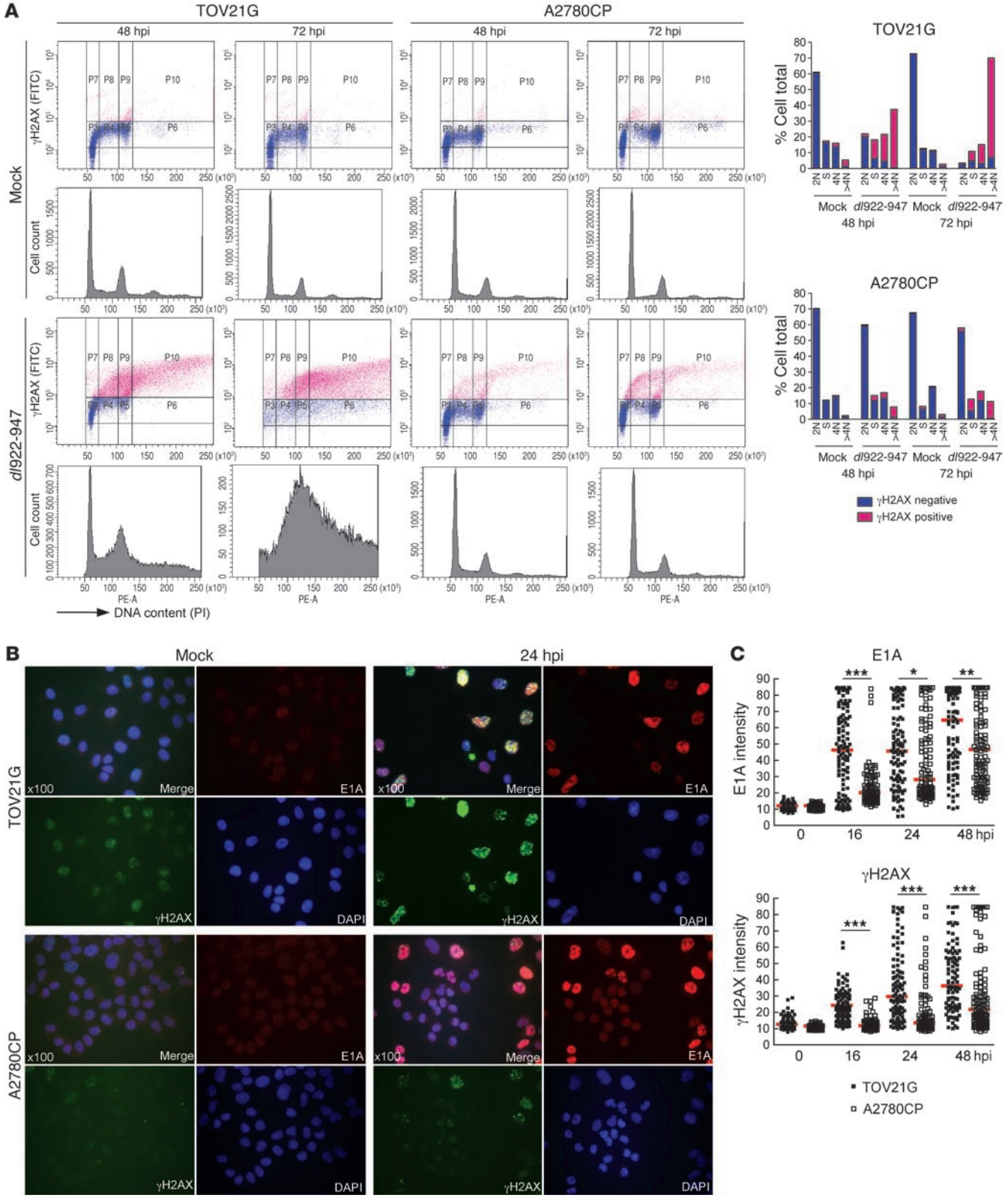
A
TOV21G
A2780CP
48 hpi
72 hpi
Mock
dl922-947
γH2AX (FITC)
Cell count
PE-A
DNA content (PI)
P3 P4 P5 P6 P7 P8 P9 P10
% Cell total
2N S 4N >4N
Mock dl922-947 Mock dl922-947
48 hpi 72 hpi
γH2AX negative
γH2AX positive
B
Mock
24 hpi
TOV21G
A2780CP
x100
Merge
E1A
γH2AX
DAPI
C
E1A
E1A intensity
γH2AX
γH2AX intensity
0 16 24 48 hpi
TOV21G
A2780CP

Figure 2
*dl*922-947 infection induces genomic DNA damage. (**A**) TOV21G and A2780CP cells were harvested after infection with *dl*922-947 (MOI 7.5), fixed in 70% cold ethanol, incubated with an anti-γH2AX antibody, counterstained with PI, and analyzed by flow cytometry. (**B** and **C**) TOV21G and A2780CP cells were fixed after infection with *dl*922-947 (MOI 7.5), stained for expression of E1A and γH2AX, counterstained with DAPI, and imaged. (**B**) Fluorescence intensity was assessed in more than 100 cells per condition using ImageJ software. Original magnification, ×100. (**C**) Each point represents a single cell, and each red bar represents the median. $^{*}P < 0.05$, $^{**}P < 0.01$, $^{***}P < 0.0001$; Mann-Whitney test.

$r = 0.832$, $P < 0.0001$, Supplemental Figure 3). BrdU-positive cells showed a pan-nuclear signal, distinct from virus replication centers, which are seen at discrete sites within the nucleus (24), supporting the association of γH2AX with genomic DNA replication. γH2AX was also detected in TOV21G cells after infection with E1A WT adenovirus, although the damage occurred more slowly than that with *dl*922-947 (Supplemental Figure 4).

Since significantly greater H2AX phosphorylation was observed in S and G_2/M cells and cells with more than 4 N DNA content, we investigated whether virus infection produced DSBs during genomic DNA replication. To analyze genomic DSBs, DNA from TOV21G and A2780CP cells was extracted up to 48 hpi, subjected to neutral pulsed-field gel electrophoresis (PFGE), and then labeled with anti-genomic DNA and anti-adenovirus type 5 DNA probes. X-irradiation (20 Gy) and TNF-related apoptosis-inducing ligand (TRAIL) (250 ng/ml) were used as positive controls for DSB and apoptotic DNA damage, respectively. *dl*922-947 induced genomic DSB damage in TOV21G cells, as indicated by the migration of genomic DNA out of the well (Figure 3A). DNA damage was initiated 24 hpi but greatly increased at 48 hpi. The intensive damage signal at approximately 50 kb is likely to represent apoptotic DNA fragmentation (25) rather than adenoviral DNA, as there is a large increase in this signal between 24 and 48 hpi in TOV21G cells but little increase in adenovirus DNA. Thus, there were different kinetics of genomic DNA damage and viral replication, which verified that infection with *dl*922-947 induces DNA damage in sensitive cells. In contrast, the resistant A2780CP cells had no genomic DNA damage compared with mock-infected controls, despite containing demonstrable adenoviral DNA. These results suggest strongly that cellular sensitivity to *dl*922-947 positively correlates with overreplication of genomic DNA and associated DNA damage.

H2AX can be phosphorylated by ATR at replication collapse (26). To investigate whether overreplication could induce ATR to activate Chk1, phosphorylation of Chk1 was examined after infection with *dl*922-947 (Figure 3B). In highly sensitive TOV21G cells, Chk1 was activated earlier than in either of the other 2 cell lines, confirming that there is functional downstream signaling in response to virus-induced genomic DNA overreplication and damage. Some later phosphorylation was seen in both IGROV1 and A2780CP cells, in keeping with the lower levels of overreplication and H2AX phosphorylation in these cells.

Chk1 inhibition augments dl922-947–induced overreplication and genomic DNA damage. To assess whether manipulation of the ATR-Chk1 pathway could influence the efficacy of adenoviruses in insensitive ovarian cancers, A2780CP cells were infected in the presence of the Chk1 inhibitor UCN-01 (7-hydroxystaurosporine; ref. 27). First, cells were harvested for cell cycle analysis up to 72 hpi. Virus or UCN-01 alone exerted no effect upon cell cycle profile, but the combination of *dl*922-947 with UCN-01 resulted in dose-dependent overreplication, leading

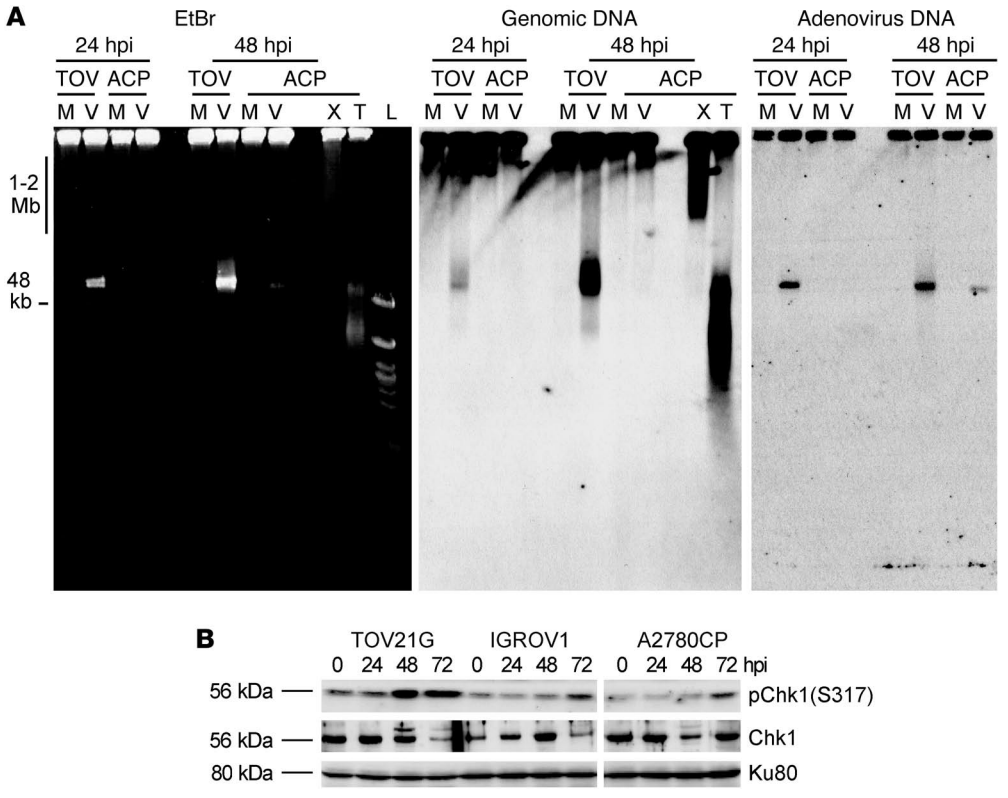

Figure 3
*dl*922-947–induced genomic DNA damage causes Chk1 phosphorylation. (**A**) TOV21G and A2780CP cells were infected with *dl*922-947 (MOI 7.5) for up to 48 hours. A2780CP cells were also treated with x-irradiation (20 Gy, 30 minutes) or TRAIL (250 ng/ml, 3 hours). DNA was extracted and subjected to neutral PFGE, stained with ethidium bromide (EtBr), and then probed with HRP-labeled genomic DNA or adenovirus type 5 probe. TOV, TOV21G; ACP, A2780CP; M, mock; V, *dl*922-947 infection; X, x-irradiation; T, TRAIL; L, Ladders. (**B**) Phosphorylation of Chk1 in TOV21G, IGROV1, and A2780CP cells infected with *dl*922-947 (MOI 7.5) for up to 72 hours was assessed by immunoblot.

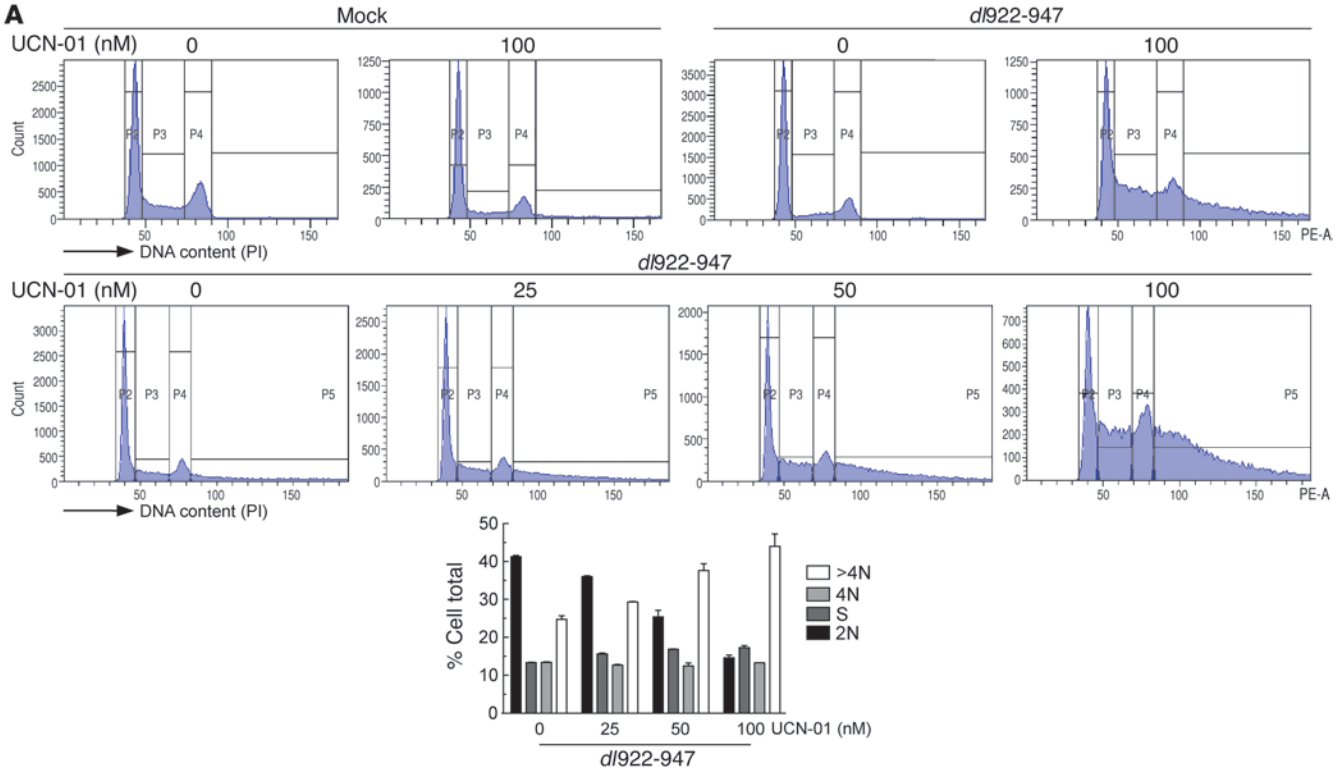

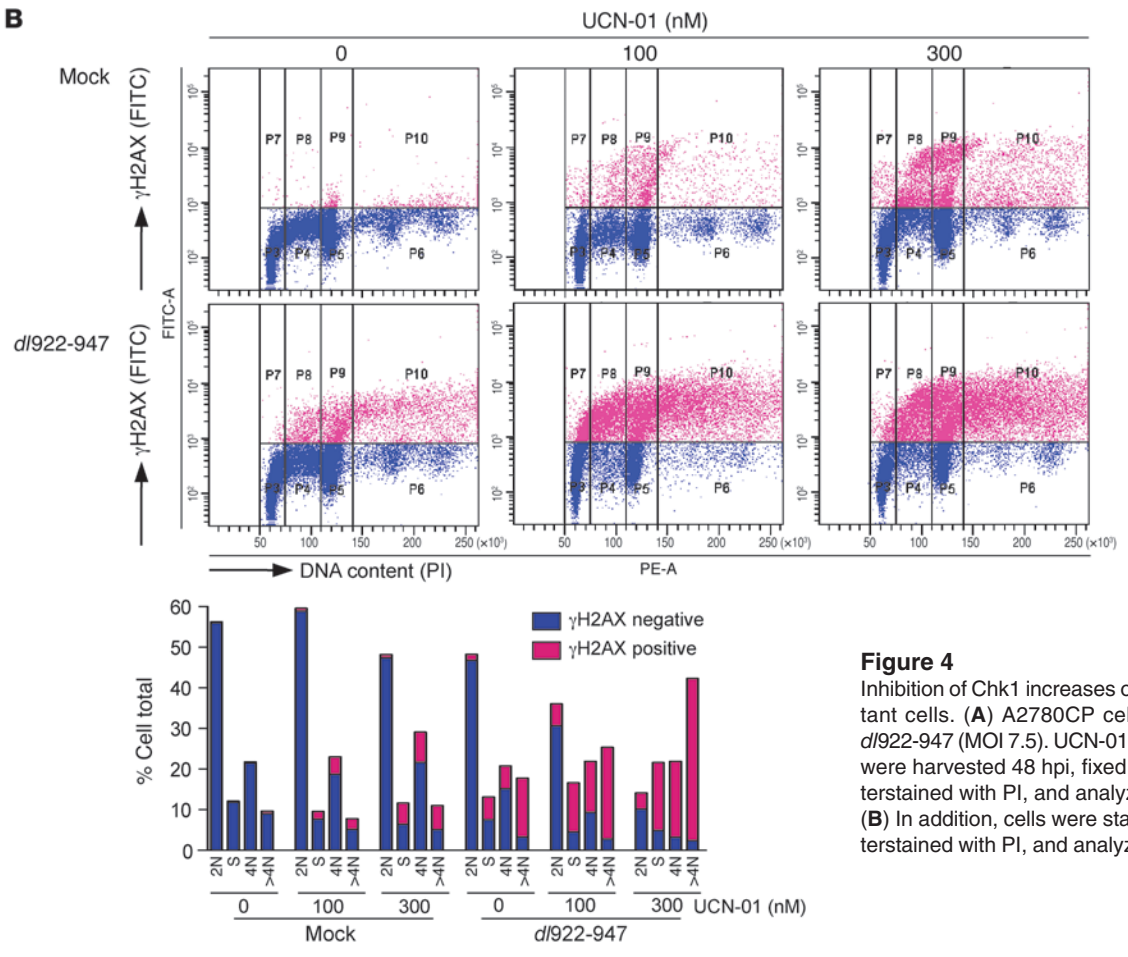

Figure 4
Inhibition of Chk1 increases overreplication in resistant cells. (**A**) A2780CP cells were infected with *dl*922-947 (MOI 7.5). UCN-01 was added 6 hpi. Cells were harvested 48 hpi, fixed in cold ethanol, counterstained with PI, and analyzed by flow cytometry. (**B**) In addition, cells were stained for γH2AX, counterstained with PI, and analyzed by flow cytometry.

to greater accumulation of cells with more than 4 N DNA content (Figure 4A). This UCN-01 effect was also seen with intermediate-sensitivity IGROV1 cells, indicating that these effects are not cell-type specific (Supplemental Figure 5). Similarly, inhibition of ATR-Chk1 signaling by siRNA-mediated knockdown of ATR induced a small but significant increase in overreplication (Supplemental Figure 6). UCN-01 also greatly enhanced γH2AX, as detected by flow cytometry (Figure 4B). Furthermore, the increase in γH2AX was most marked in S/G_2 and overreplicated cells; treatment of cells with UCN-01 alone in the absence of virus infection had no effect upon the proportion of overreplicated cells. However, the combination of *dl*922-947 and 300 nM UCN-01 increased the proportion of overreplicated cells from 11% (UCN-01 alone) and 17% (*dl*922-947 alone) to 42.3% (combination), with over 89% of the cells with more than 4 N DNA content being γH2AX positive. By comparison, under 10% of G_1 phase cells were γH2AX positive, despite receiving the same treatment. Importantly, UCN-01 did not induce overreplication in primary human fibroblast cells after infection with either *dl*922-947 or Ad5 WT, implying that the effects of Chk1 inhibition on viral function are specific to malignant cells (Supplemental Figure 7).

IF analysis of γH2AX and E1A intensity in A2780CP cells after infection with *dl*922-947 indicated that 300 nM UCN-01 slightly increased the median intensity of E1A per cell from 11.5 to 15.6 relative fluorescence units (RFU) (Figure 5A; $P = 0.02$) but induced a greater proportional increase in γH2AX: there was no difference in the median intensity of γH2AX staining after UCN-01 and *dl*922-947 given individually (9.9 and 9.5 RFU, respectively), but the combination caused a highly significant increase to 35.7 RFU ($P < 0.0001$). Thus, inhibition of Chk1 augmented the accumulation of γH2AX following E1A expression, an effect that was also seen in IGROV cells (data not shown). To confirm that this effect was Chk1 specific, IGROV1 cells were transfected with siRNA to Chk1 prior to infection with *dl*922-947. IF demonstrated a significant increase in γH2AX formation compared with that in control cells 24 hpi at 2 MOIs (Figure 5B).

To analyze directly the effect of Chk1 inhibition and associated overreplication upon genomic DNA damage, DNA was extracted from A2780CP cells after infection and subjected to neutral PFGE. Treatment with UCN-01 or *dl*922-947 alone induced modest DNA damage, but the combination of UCN-01 and *dl*922-947 induced large numbers of genomic DSBs in a UCN-01 concentration–dependent manner (Figure 5C). Labeling with an adenovirus DNA probe confirmed that, as in Figure 3A, the large band at approximately 50 kb seen in the genomic DNA blot does not correspond to adenoviral DNA, despite the similar size, and also that UCN-01 treatment does not compromise viral DNA replication.

Chk1 inhibition decreases HR repair in dl922-947–treated cells. Replication-associated DNA breaks are preferentially repaired via the HR pathway (28). In response to such breaks, activated Chk1 is responsible for recruitment of Rad51, which in turn catalyses the homology search and DNA strand exchange functions that are central to HR (reviewed in ref. 29). To examine how Chk1 inhibition alters HR repair after *dl*922-947 infection, we quantified Rad51 focus formation by IF in A2780CP cells. *dl*922-947 infection alone caused a significant increase in the number of Rad51-positive cells, but there was a significant and dose-dependent reduction in Rad51 positivity in the presence of UCN-01 (Figure 6). Collectively, the results in Figures 4–6 demonstrate that inhibition of Chk1 increases overreplication with extensive DNA damage and prevention of HR pathway activation.

Chk1 inhibition augments adenovirus activity in vitro and in vivo. The overreplication and genomic DNA damage effects induced by UCN-01 caused a dose-dependent increase in cytotoxicity of both *dl*922-947 and Ad5 WT in both A2780CP and IGROV1 cells (Figure 7A and data not shown). In addition, UCN-01 did not impede the production of intracellular infectious virions and caused an increase in virus release, possibly due to increased cell death and lysis (Figure 7B). siRNA-mediated Chk1 knockdown was highly toxic, such that it was not possible to maintain cells alive for the duration of a cytotoxicity assay. However, to demonstrate further that the effects were specific to Chk1, both A2780CP and IGROV1 cells were infected with *dl*922-947 or Ad5 WT in the presence of the Chk1 inhibitor PF-00477736 (30). Sensitivity to both viruses was increased in both cell lines (Figure 7C).

To investigate whether these effects translated into increased antitumor activity in vivo, female nude mice bearing size-matched subcutaneous IGROV1 tumors received a single intratumoral injection of *dl*922-947 (10^{10} particles), with or without a single dose of UCN-01 (7.5 mg/kg) i.p. 24 hours later. Tumors were harvested 48 hours after virus. Greater E1A was detected in tumors from mice treated with *dl*922-947 and UCN-01 compared with those treated with *dl*922-947 and vehicle (Figure 7D). Mice bearing established IGROV1-luciferase i.p. xenografts were then treated with *dl*922-947 and UCN-01 alone and in combination. UCN-01 and *dl*922-947 given individually caused tumor stasis, as monitored by bioluminescence imaging, whereas combination treatment caused significant tumor regression, which was sustained until the end of the experiment (Figure 7E). In A2780CP xenografts, UCN-01 and *dl*922-947 alone had no therapeutic effect, whereas the combination again caused regression, although this was temporary (data not shown).

Cdc25A is a key regulator of adenovirus cytotoxicity. To understand how Chk1 inhibition can promote overreplication, increase DNA damage, and augment viral activity, we investigated the Chk1 target Cdc25A. Cdc25A is a target of E1A transactivation during adenovirus infection and promotes E1A-induced S phase entry (31). Deregulated Cdc25A phosphatase activity is sufficient to induce unscheduled genomic DNA replication through activation of cyclin-dependent kinases (32, 33). During an unperturbed interphase, Cdc25A is subject to basal physiological turnover, which is accelerated in response to genotoxic damage (34), mediated by the ATR-Chk1 pathway (35, 36). To investigate a possible link between Chk1, Cdc25A, and cellular sensitivity, Cdc25A expression was assessed after infection with *dl*922-947. As with E1A, virus-induced Cdc25A expression was greater in TOV21G cells than in the insensitive cells (Figure 8A), which resulted predominantly from increased transcription (Supplemental Figure 8A). An increase in transcription was observed in both IGROV1 and A2780CP cells at higher MOIs (Supplemental Figure 8B), suggesting a possible threshold effect. A2780CP cells were then infected with *dl*922-947 for 48 hours in the presence and absence of UCN-01. Cdc25A was degraded via a ubiquitin-proteasome-dependent pathway, and the combination of *dl*922-947 and the proteasome inhibitor MG132 caused a very marked increase in Cdc25A levels (Figure 8B), indicating that Cdc25A is targeted for proteasome-dependent degradation in insensitive A2780CP cells after *dl*922-947 infection. Chk1 inhibition with UCN-01 stabilized Cdc25A, with a very marked increases in γH2AX (Figure 8B). There was also an increase in E1A (Figure 8C), which complemented the IF and overreplication data (Figures 4 and 5) and the immunohistochemistry from IGROV1 tumors (Figure 7D) and substantiated Chk1 as a mediator of

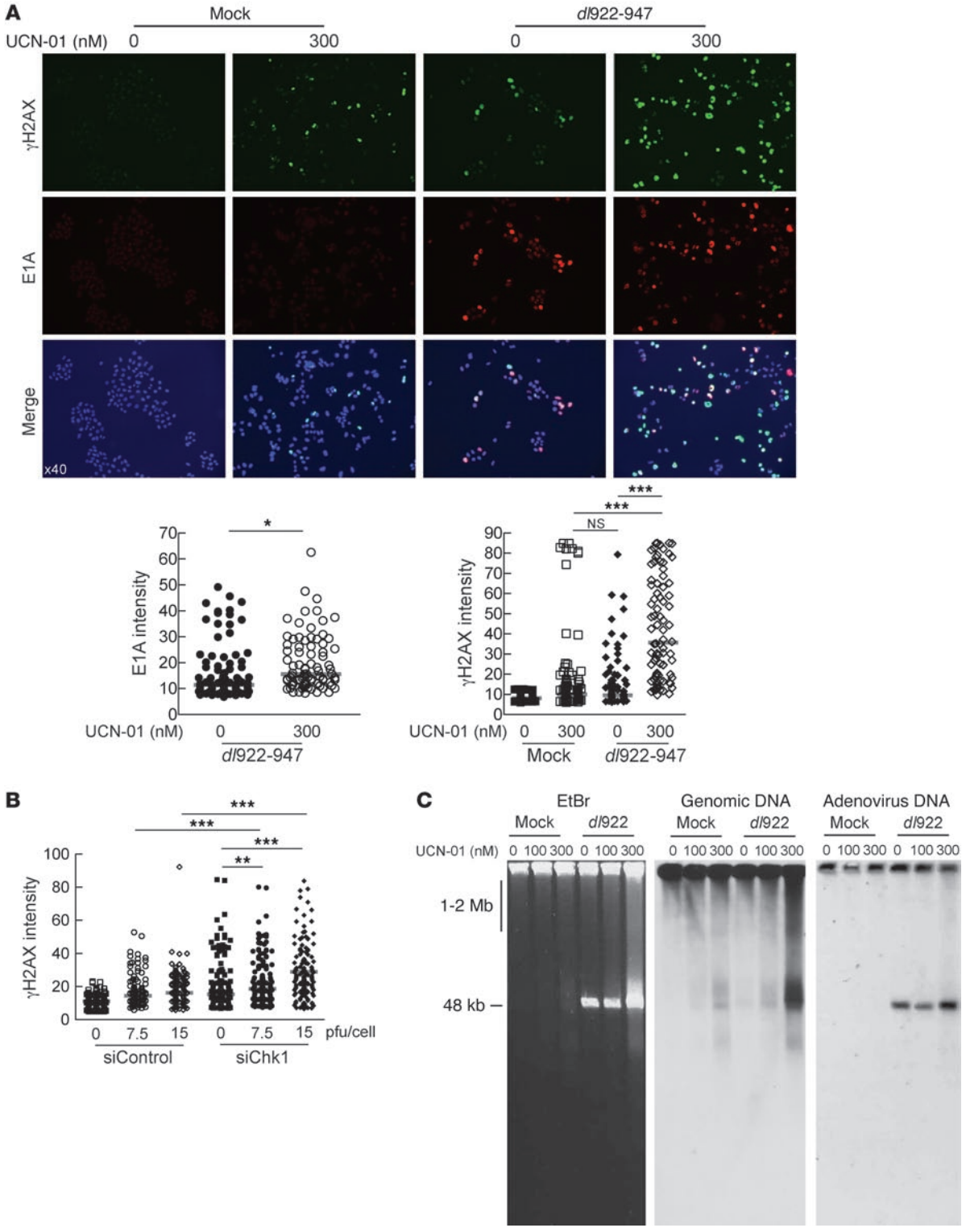

Figure 5

Loss of Chk1 activity increases genomic DNA damage. (**A**) A2780CP cells were infected with *dl*922-947 (MOI 7.5) and treated with UCN-01 6 hours later. 48 hpi, cells were fixed, stained for expression of E1A and γH2AX, counterstained with DAPI, and imaged. Fluorescence intensity was assessed in more than 100 cells per condition using ImageJ software. Each point represents a single cell, and each red bar represents the median. Original magnification, ×40. *$P < 0.05$, ***$P < 0.0001$; Mann-Whitney test. (**B**) IGROV1 cells were transfected with Chk1 (siChk1) or scrambled control siRNA (siControl) oligonucleotides 24 hours prior to infection with *dl*922-947 (MOI 7.5 and 15). Cells were fixed 24 hours thereafter, stained for expression of γH2AX, and counterstained with DAPI. Fluorescence intensity was assessed as before. **$P < 0.01$, ***$P < 0.0001$; Mann-Whitney test. (**C**) A2780CP cells were infected with *dl*922-947 (MOI 7.5) for 48 hours, with or without treatment with UCN-01. DNA was extracted and subjected to neutral PFGE and probed with HRP-labeled genomic DNA or adenovirus type 5 probe.

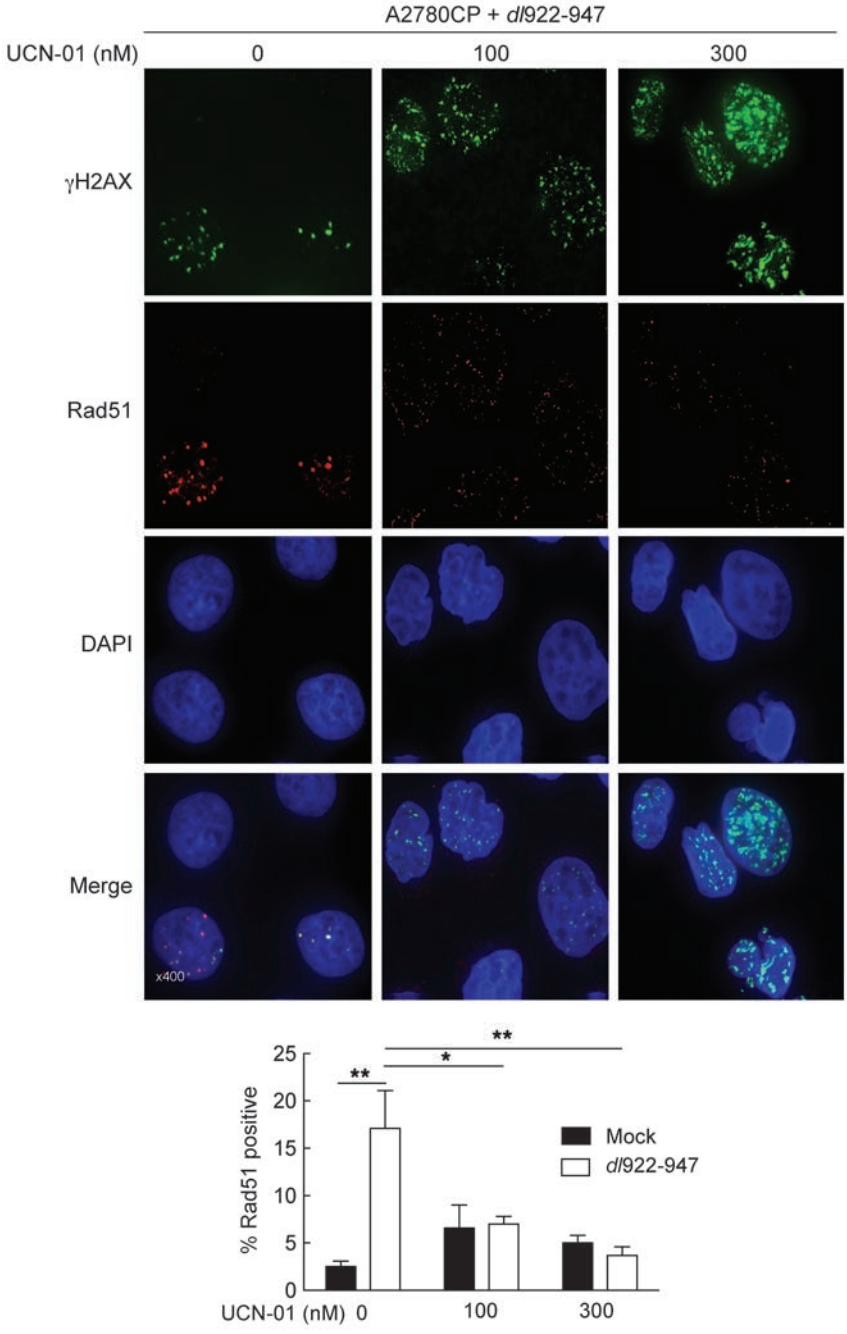

Figure 6
UCN-01 reduces HR DNA repair. A2780CP cells were infected with *dl*922-947 (MOI 7.5) and treated with UCN-01 6 hours later. 48 hpi, cells were fixed, stained for expression of γH2AX and Rad51, counterstained with DAPI, and imaged. Original magnification, ×400. The numbers of Rad51-positive (>10 foci) nuclei in 10 fields of view were counted. $^{*}P < 0.05$, $^{**}P < 0.01$.

Cdc25A degradation. The increase in Cdc25A with UCN-01 did not result from increased transcription (data not shown), confirming that Cdc25A stabilization occurs posttranscriptionally. MG132 did not increase virus-induced H2AX phosphorylation, because adenovirus function depends critically upon proteasomal degradation of key cellular proteins, including p53 (37).

siRNA-mediated ATR knockdown was also able to stabilize Cdc25A after *dl*922-947 infection (Figure 8D), in contrast to the ATM inhibitor 2-morpholin-4-yl-6-thianthren-1-yl-pyran-4-one (data not shown), confirming the involvement of the ATR-Chk1 pathway. Finally, overexpression of Cdc25A significantly increased virus cytotoxicity in both A2780CP cells (Figure 8E) and IGROV1 cells (data not shown), with increased γH2AX formation (Figure 8E). Conversely, Cdc25A knockdown reduced virus-induced DNA damage in TOV21G cells (Figure 8F) and also reversed both the DNA damage and overreplication seen in A2780CP cells treated with UCN-01 after virus infection (Figure 8G). These results substantiate Cdc25A as an important mediator of virus-induced DNA damage and as a key target for Chk1 activity after infection.

Overall, we propose a model whereby the sensitizing effects of Chk1 inhibition upon adenovirus-induced cell death in cancer cells are compound (Figure 9). These include (a) prevention of Chk1-mediated degradation of Cdc25A, which promotes unscheduled DNA synthesis with consequent induction of DNA damage, and (b) inhibition of Chk1-mediated recruitment of Rad51 to DSBs, which impairs HR repair. Together, these effects expedite the accumulation of cytotoxic lesions and cell death after infection.

Discussion

The mode of adenovirus-induced cell death has remained obscure (7) and thereby difficult to manipulate for therapeutic gain. Unscheduled DNA synthesis induces the accumulation of replication-associated DNA lesions (11, 21, 38), and our data support a correlation between adenovirus-induced genomic DNA overreplication and cytotoxicity in ovarian cancer. We demonstrate that the E1A-CR2 mutant adenovirus *dl*922-947 induced massive accumulation of genomic DNA damage, specifically in cell lines sensitive to adenovirus-induced cell death. Similar DNA damage was also induced in sensitive cells by the WT adenovirus, although this occurred more slowly. The damage, in the form of DSBs, occurred predominantly and specifically in replicating cells and was most prominent in those cells harboring a more than 4 N DNA content, consistent with DNA damage being dependent upon aberrant overreplication of genomic DNA. As a consequence, DSBs were less abundant in resistant cells, in which there was minimal overreplication after infection.

Sensitive cells support greater transcription of E1A in the first hours after infection. Similarly, sensitive cells permit transcription of Cdc25A early after infection, which promotes G_1/S transition by dephosphorylating, and thereby activating, cyclin A- and cyclin E-cdk2 kinases, which are the rate limiting factors for firing of DNA replication origins. Transactivation of Cdc25A

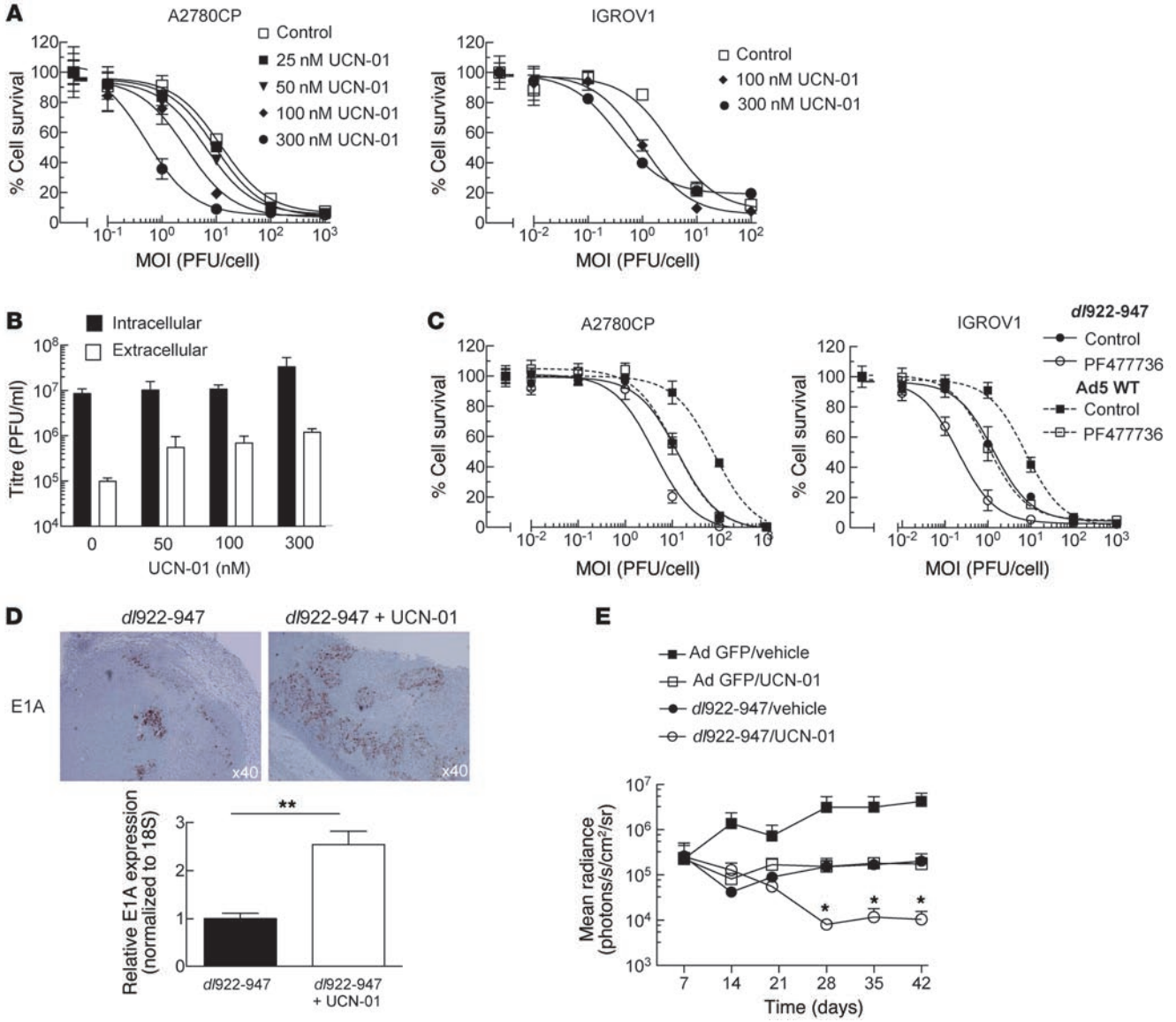

Figure 7

UCN-01 increases *dl*922-947 activity in vitro and in vivo. (**A**) A2780CP and IGROV1 cells were infected with *dl*922-947. UCN-01 was added 6 hpi. Cell survival was assessed 120 hpi. (**B**) A2780CP cells were harvested 72 hours after *dl*922-947 (MOI 7.5) infection and treatment with UCN-01. Titers of intracellular and extracellular adenovirus were assessed by $TCID_{50}$. (**C**) A2780CP and IGROV1 cells were infected with *dl*922-947 or Ad5 WT. PF477736 (360 nM for A2780CP, 120 nM for IGROV1) was added 6 hpi. Cell survival was assessed 120 hpi. (**D**) *dl*922-947 (10^{10} particles) was injected into subcutaneous IGROV1 xenografts on the flank of athymic *nu*/*nu* female mice. 24 hpi, mice received a single i.p. dose of UCN-01 (7.5 mg/kg) or vehicle (20% icodextrin). Mice were killed 24 hours thereafter. Expression of E1A was assessed by immunohistochemistry (top). RNA was extracted from snap frozen tumors, and E1A expression was assessed by qRT-PCR (bottom). Expression was normalized to that of 18S RNA and plotted relative to mice that received *dl*922-947 and vehicle. Original magnification, ×40. $^{**}P < 0.01$. (**E**) 5×10^6 IGROV1-luciferase cells were injected i.p. into athymic *nu*/*nu* female mice. On day 9, mice were randomly allocated to receive i.p. *dl*922-947 or control adenovirus (5×10^9 particles/day on days 9, 10, 15, and 16), with or without i.p. UCN-01 (5 mg/kg on days 11, 12, 17, and 18). Tumor burden was assessed using bioluminescence imaging. Bars represent SEM; $n = 5$/group. $^{*}P < 0.05$, for 1-tailed comparison of *dl*922-947/UCN-01 versus both adenovirus GFP/UCN-01 and *dl*922-947/vehicle.

through 2 functional E2F-binding sites (E2F-A and E2F-C) within the Cdc25A promoter is essential for efficient induction of S phase by E2F1 and pRb family members (39). Cdc25A also promotes E1A-mediated S phase entry and DNA synthesis following after with adenovirus (31). Previously, it was reported that E1A expression was not responsible for γH2AX formation in HeLa cells after adenovirus infection: widespread γH2AX was seen only after infection with WT virus and not a nonreplicating pTP-deleted virus. In these experiments, E1A expression was seen with both viruses but at greater levels with the WT virus (16). However, we found a good correlation between E1A expression and appearance of γH2AX across cell lines. Our data suggest that

there may be a threshold effect, whereby E1A expression must reach a threshold level to induce sufficient Cdc25A to promote genomic DNA overreplication (31). Thus, rapid genomic overreplication and DNA damage are seen in TOV21G cells but at much lower levels in resistant and partially sensitive cells and only once E1A expression reaches a level sufficient to transactivate Cdc25A or after infection at much greater MOI.

Inhibition of ATR-Chk1-Cdc25A pathway augments dl922-947 cytotoxicity via 2 mechanisms

In our model (Figure 9), we suggest that Chk1 inhibition increases virus cytotoxicity via 2 separate mechanisms.

Increase in overreplication via Cdc25A stabilization. Cdc25A is subject to proteasome-dependent degradation mediated by the ATR-Chk1 pathway. This acts to modulate the pro-replicative activity of cyclin E-cdk2 during an unperturbed cell cycle (35). Replication-associated DNA damage intensifies ATR-Chk1 signaling, which accelerates Cdc25A degradation to enact S phase checkpoint control (35, 40). As a consequence, downregulation of either ATR or Chk1 activity results in accumulation of Cdc25A and deregulated DNA synthesis (40). The increase in overreplication was less marked with ATR knockdown than with UCN-01–mediated Chk1 inhibition, which may simply reflect difficulty in achieving complete knockdown. We failed to detect accumulation of Cdc25A in uninfected cells after either ATR siRNA (data not shown) or Chk1 inhibition with UCN-01 (Figure 8C) but did so only with *dl*922-947 infection. The increased Cdc25A levels seen with Chk1 inhibition in infected cells were achieved despite no increase in Cdc25A transcription but were still sufficient to promote overreplication. The overreplication promoted the formation and accumulation of genotoxic DNA lesions to sensitize these otherwise resistant cells to *dl*922-947–induced cell death. Further evidence for a role for Cdc25A was provided by overexpression, which increased DNA damage and cytotoxicity in A2780CP cells, while, conversely, Cdc25A knockdown not only reduced virus-induced DNA damage in TOV21G cells but also reversed the overreplication promoted by UCN-01 in A2780CP cells. One question is how TOV21G cells can maintain Cdc25A expression (Figure 8A) in the presence of active phospho-Chk1 (Figure 3B). The levels of Cdc25A after infection will reflect the balance between virus-induced expression and Chk1-mediated degradation. In TOV21G cells, E1A levels were sufficient to overcome the effects of Chk1 — indeed, Chk1 inhibition in TOV21G cells increased their overreplication even further (data not shown).

Augmentation of DNA damage by preventing HR repair. There is evidence that adenovirus infection can inhibit certain forms of DNA damage repair: the E1B55K/E4orf6 complex promotes the degradation of DNA ligase IV, which is vital to the process of nonhomologous end-joining (41). However, replication-associated DSBs are preferentially repaired by HR, in which Rad51 is a key mediator (reviewed in ref. 29). Phosphorylation of Rad51 by Chk1 promotes the chromatin association of Rad51 and is required for efficient HR repair and survival after replication stress-induced DNA damage (36). Interestingly, we detected Rad51 foci as well as γH2AX signal after infection with *dl*922-947, indicating that *dl*922-947–induced DSBs activate both DNA damage and DNA repair signaling. We demonstrate that inhibition of Chk1 activity with UCN-01 reduced the formation of Rad51 foci after infection, implying that UCN-01 also impacts on adenovirus-induced signaling to ATR-Chk1-Rad51–directed HR repair.

Our data also suggest strongly that cell sensitivity to virus-induced cytotoxicity is not a direct function of intracellular virion load: the number of viral genomes and functional virions was similar in all 3 cell lines examined here, despite their widely differing sensitivity to virus cytotoxicity. Moreover, UCN-01 treatment increased cell death without any substantial increase in the number of intracellular virions.

The factors that determine cellular sensitivity to adenovirus-mediated cytotoxicity are likely to be legion. We have recently demonstrated that expression of p21 in ovarian cancer is a marker for a host cell environment conducive to the expression of E1A (8). *E1A* is the first viral gene to be expressed after infection, and its expression correlates with cellular sensitivity. The data presented here indicate that the cellular environment can also impact on events downstream of E1A expression and, furthermore, can be instrumental in the ultimate fate of a cell. In addition, the ease of virus spread between infected cells will contribute to overall cell sensitivity. Spread relies both upon release of virus from initially infected cells as well as upon subsequent infection of neighboring cells. Although adenovirus release is largely lytic, we have recently shown that a nonlytic mechanism may exist, dependent upon stabilized microtubules (42). The in vitro experiments described here lasted for 5 days at most, which allowed approximately 2–3 rounds of replication (43). It will therefore be important to investigate the patterns of DNA damage and cytotoxicity in ovarian cancer cells after infection at a lower MOI, which will demand multiple rounds of replication and release.

Two major questions remain. First, why are the changes greater after *dl*922-947 infection compared with those after WT adenovirus infection? *dl*922-947 has greater cytotoxicity than Ad5 WT in a variety of cancer models (2, 3), which has been demonstrated again here. However, the molecular origin of this increased activity is uncertain. The data presented here indicate that the superior activity of *dl*922-947 mirrors the increased DNA damage and overreplication. The 24-bp deletion within E1A-CR2 region in *dl*922-947 greatly reduces binding to host cell p107, pRb, and cyclin A (1), effects that correlate with reinitiation of DNA synthesis and host cell overreplication (44) as well as induction of cdk1 activity (45). Thus, the superior potency of *dl*922-947 may be caused by uncoordinated host cell DNA replication, with consequent activation of DNA damage responses. Second, what is the role of HR competence in repairing virus-induced genomic DNA damage? There is much interest in the role of HR incompetence as a predictor of ovarian cancer responsiveness to PARP inhibition (38, 46, 47). Our data would suggest that HR incompetence would predispose cells to adenovirus-induced cell death, while inhibiting HR in HR-proficient cells could convey sensitivity to otherwise resistant cells. We are currently exploring both questions further.

In summary, our data demonstrate that mechanisms to promote unscheduled DNA synthesis and/or impede HR repair will potentiate the accumulation of cytotoxic lesions and increase death induced by the oncolytic adenovirus *dl*922-947. As UCN-01 has already shown itself to be safe in patients with advanced ovarian cancer (48), combination trials with oncolytic viruses should be explored.

Methods

Cell culture, adenoviruses, and cell viability assays. All cells were maintained at 37°C with 5% CO_2, in Dulbecco's modified Eagle's medium supplemented with 10% FCS, penicillin/streptomycin, and fungizone. *dl*922-947 is an adenovirus type 5 mutant containing a 24-bp deletion in E1A-CR2, which is also deleted in E3B. *dl*309 is identical to *dl*922-947 apart from a WT E1A region. Control

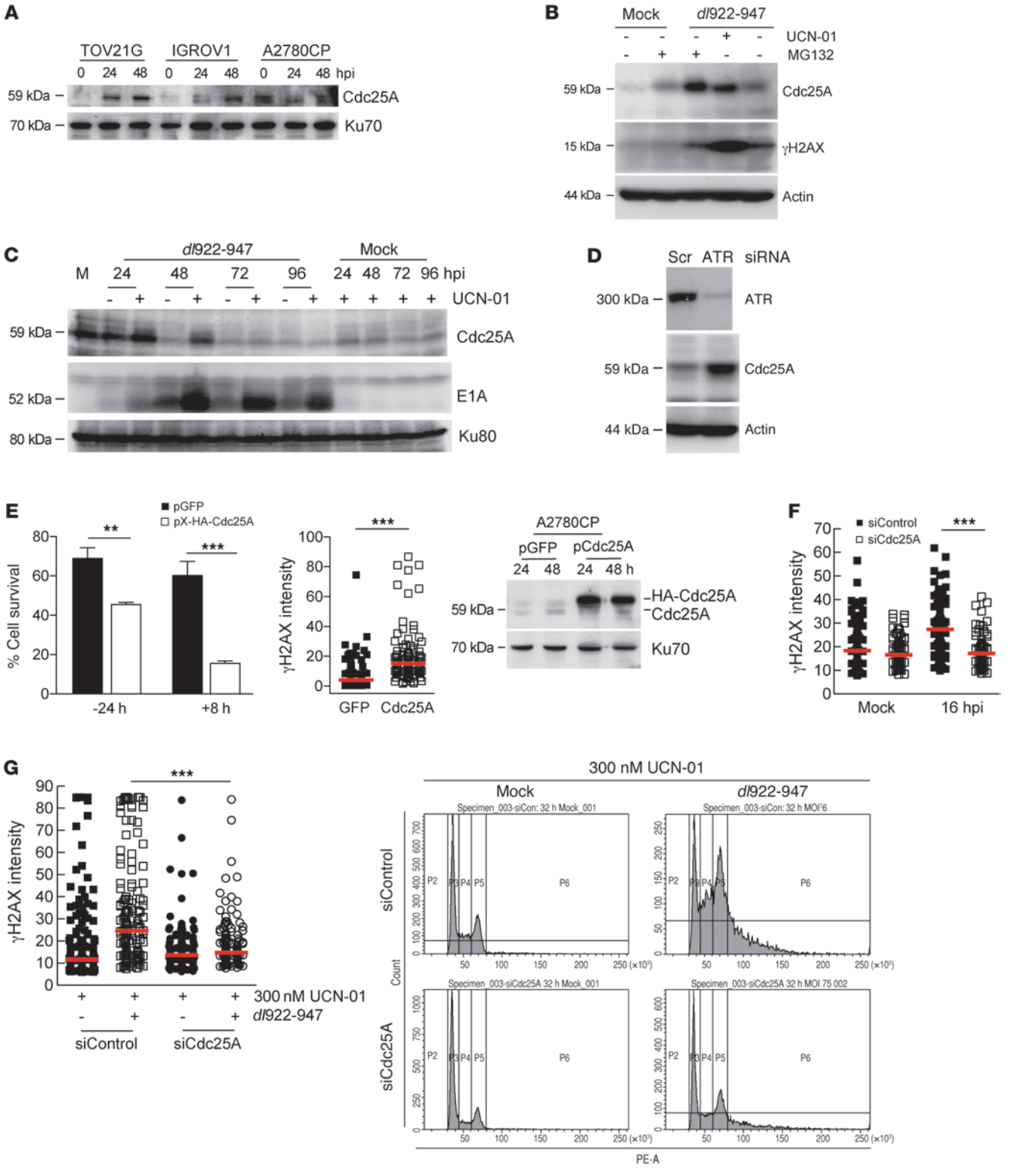
A
TOV21G
IGROV1
A2780CP
0 24 48 0 24 48 0 24 48 hpi
59 kDa
Cdc25A
70 kDa
Ku70
B
Mock
dl922-947
UCN-01
MG132
59 kDa
Cdc25A
15 kDa
γH2AX
44 kDa
Actin
C
dl922-947
Mock
M 24 48 72 96 24 48 72 96 hpi
UCN-01
59 kDa
Cdc25A
52 kDa
E1A
80 kDa
Ku80
D
Scr ATR siRNA
300 kDa
ATR
59 kDa
Cdc25A
44 kDa
Actin
E
pGFP
pX-HA-Cdc25A
% Cell survival
-24 h
+8 h
γH2AX intensity
GFP Cdc25A
A2780CP
pGFP pCdc25A
24 48 24 48 h
59 kDa
HA-Cdc25A
Cdc25A
70 kDa
Ku70
F
siControl
siCdc25A
γH2AX intensity
Mock
16 hpi
G
γH2AX intensity
300 nM UCN-01
dl922-947
siControl
siCdc25A
300 nM UCN-01
Mock
dl922-947
siControl
siCdc25A
Count
PE-A

Figure 8
Cdc25A is a key regulator of adenovirus cytotoxicity. (**A**) Cdc25A expression was assessed by immunoblot after *dl*922-947 infection (MOI 7.5). (**B** and **C**) A2780CP cells infected with *dl*922-947 were treated with UCN-01 (300 nM) or MG132 (10 μM) and harvested 48 hpi. (**B**) Cdc25A and γH2AX expression 24 hpi and (**C**) E1A expression up to 96 hpi were assessed by immunoblot. (**D**) 24 hours after transfection with ATR-specific siRNA or scrambled control (Scr), A2780CP cells were infected with *dl*922-947 (MOI 7.5). ATR and Cdc25A expression was assessed by immunoblot 72 hpi. (**E**) A2780CP cells were transfected with pX-HA-Cdc25A or pGFP 24 hours before (–24 hours) or 8 hours after (+8 hours) infection with *dl*922-947 MOI 100. Cell survival was assessed 96 hpi (left). $^{**}P < 0.01$, $^{***}P < 0.001$. γH2AX expression was also assessed in cells infected with *dl*922-947 and transfected 8 hours later with pX-HA-Cdc25A (middle). Red bars represent median. $^{***}P < 0.0001$; Mann-Whitney test. Expression of HA-tagged Cdc25A was confirmed by Cdc25A immunoblot (right). (**F**) TOV21G cells were transfected with Cdc25A-specific siRNA or scrambled control, infected with *dl*922-947 (MOI 7.5 and 15) later and stained for γH2AX expression 16 hours thereafter. Red bars represent median. $^{***}P < 0.0001$; Mann-Whitney test. (**G**) A2780CP cells were transfected with Cdc25A-specific siRNA or scrambled control 24 hours prior to infection with *dl*922-947 (MOI 7.5). Cells were additionally treated with UCN-01 6 hpi and fixed 24 hpi. γH2AX expression (left) and flow cytometry (right) were performed as before. Red bars represent median. $^{***}P < 0.0001$; Mann-Whitney test.

viruses adenovirus CMV GFP and adenovirus LM-X are both E1-deleted nonreplicating vectors as previously described (49). For viability assays, 2×10^4 cells were infected in serum-free medium at MOI 0.001–1,000 PFU/cell. After 2 hours, cells were refed with medium containing 5% FCS. Cell viability was assayed by MTT assay using a Victor3 Plate Reader (Perkin Elmer). All viability assays were done in triplicate, and experiments were repeated at least twice. For siRNA experiments, cells were transfected with ON-TARGETplus SMARTpool siRNAs or scrambled siRNA control (Dharmacon) using DharmaFECT1. Virus infection took place 24 hours after knockdown. Cells were exposed to 5 Gy X-irradiation using an Hs-X-Ray System (A.G.O. Installations Ltd.). ATM inhibitor 2-morpholin-4-yl-6-thianthren-1-yl-pyran-4-one was obtained from Calbiochem. The plasmid pX-HA-cdc25a was donated by Ingrid Hoffman (German Cancer Research Center, Heidelberg, Germany) (33), and pGFP was obtained from Invitrogen. Plasmids (1 μg) were transfected into cells in 24-well plates using FuGene (Roche).

Quantitative PCR and $TCID_{50}$ assays. Real-time PCR was performed on an ABI Prism 7700 (Applied Biosystems). Oligonucleotides and probes for E1A and β-actin are as follows: E1A, sense primer, 5′-CCACCTACCCTTCACGAACTG; anti-sense primer, 5′-GCCTCCTCGTTGGGATCTTC; probe, ATGATTTAGACGTGACGGCC; and β-actin, sense primer, 5′-GCCAGCTCACCATGGATGAT; anti-sense primer, 5′-CACCTCCCCTGTGTGGACTT; probe, AGGCGGACTATGACTTAGTTGCGTACACCCT.

Those for 18S RNA and Cdc25A were purchased from Applied Biosystems (reference numbers 4310893E and Hs00947998_m1, respectively). PCR conditions were as follows: 50°C for 2 minutes and 95°C for 10 minutes, followed by 40 cycles of 95°C for 15 seconds and 60°C for 60 seconds. Where stated, a standard curve using 10^3–10^9 *dl*922-947 genomes was used for quantification.

Figure 9
Proposed mechanism for role of DNA damage and Chk1 inhibition in *dl*922-947 cytotoxicity. (i) Inhibition of Chk1-mediated degradation of Cdc25A promotes unscheduled DNA synthesis, with consequent induction of DNA damage. (ii) Inhibition of Chk1 activity prevents recruitment of Rad51 to DSBs, which impairs HR repair. These mechanisms expedite the accumulation of cytotoxic lesions and ensuing cell death after infection.

For tissue culture infectious dose 50% ($TCID_{50}$) assays, 10^5 cells were infected at MOI 7.5 PFU/cell. Cells were harvested into 0.5 ml 0.1 M Tris, pH 8.0, and subjected to 3 rounds of freeze/thawing (liquid N_2/37°C), after which they were centrifuged. The supernatant was titered on JH293 cells by serial dilution. To assay viral release from infected cells, culture medium was removed from cells every 24 hours and titered separately on JH293 cells.

Immunoblotting and IF. Protein lysates were electrophoresed on SDS-polyacrylamide gels and transferred onto nitrocellulose membranes by semidry blotting. Antibody binding was visualized using enhanced chemiluminescence (GE Healthcare). Antibodies used were anti-E1A, anti-Cdc25A, anti-ATR, anti-Actin, and anti-Ku70 (all Santa Cruz Biotechnology Inc.); anti-γH2AX (Upstate Biotechnology); anti-Ser 317 phospho-Chk1 (Cell Signaling Technology); anti-PARP (Serotec); and anti-Ku-80 (gifted from the lab of Penny Jeggo, University of Sussex). For IF, cells were grown on poly-L-lysine–coated coverslips, infected with *dl*922-947 (MOI 7.5), and fixed with 5% formaldehyde. Cells were permeabilized with 0.15% Triton X-100, and primary antibody binding was visualized with Texas Red– or Fluorescein-conjugated secondary antibodies (Vector Laboratories). For Rad51 staining, cells were preextracted with 0.15% Triton X-100 and fixed with 5% formaldehyde. Coverslips were mounted in DAPI-containing Vectashield and imaged using either a Zeiss Axioplan2 or a Zeiss Axiovert 200M fluorescence microscope with a ×4 or ×10 objective lens and a digital camera (Orca-ER, Hamamatsu) and Delta Vision Spectris software, with a ×100 objective lens for Rad51 foci (Applied Precision). Images taken at ×40 magnification were processed using Simple PCI software, and signal intensity per nucleus was analyzed using NIH ImageJ (http://rsbweb.nih.gov/ij/).

Flow cytometry. For cell cycle analyses, cells were trypsinized, washed twice in ice-cold PBS, and fixed in 70% ethanol. Cells were then washed with PBS and resuspended in 200 μl trypsinized PI and 100 μg/ml RNase A (MP Biomedicals). For γH2AX analysis, cells were harvested, washed, and fixed in ice-cold 70% ethanol. After incubation with primary anti-γH2AX mAb and FITC-conjugated anti-mouse secondary antibody for 20 minutes each at 37°C in the dark, cells were counterstained with PI. Cells were analyzed using a Fluorescence Activated Cell Sorter (FACSCanto, BD Biosciences), with FACS Diva software.

PFGE. Cells were infected with *dl*922-947 (MOI 7.5), with or without treatment with UCN-01. After trypsinization, cells were washed twice with PBS and were embedded in 0.75% low melting agarose gel plug (SeaPlaque agarose, Cambrex Bioproducts) at a concentration of 0.75×10^5 cells/plug. Plugs were then placed in buffer containing 20 mg/ml proteinase K, 0.5 M EDTA, and 1% sarkosyl (pH 9.0) and incubated at 50°C for 24 hours in the dark. Plugs were washed with 50 mM EDTA at room temperature for 1 hour and stored at 4°C in the same buffer. PFGE was carried out a CHEF Mapper (Bio-Rad), with a cooling module (Model 1000 Mini Chiller, Bio-Rad) in

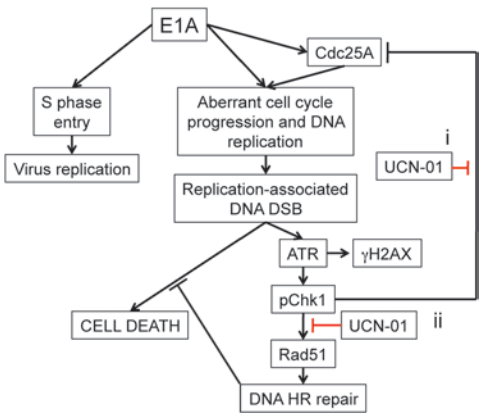

1% agarose gel (Pulsed Field Certified Agarose, Bio-Rad) in 0.5 × TBE. The forward voltage gradient was 5.4 V/cm for 5 to 60 seconds, and the reverse voltage gradient was 3.6 V/cm for 5 to 60 seconds, for a total of 20 hours at 14°C. After PFGE, gels were stained with ethidium bromide and photographed under UV transillumination. Southern blot hybridization was carried out using standard procedures with HRP-conjugated genomic DNA or adenovirus type probes.

In vivo analyses and immunohistochemistry. Experiments were performed under suitable United Kingdom Home Office personal and project license authority. All animal studies were also reviewed and approved by the ethical review board of the Biological Services Unit, Queen Mary University of London.

For analysis of E1A expression, 5×10^6 IGROV1 cells were inoculated subcutaneously onto the flank of female *nu/nu* mice on day 1. Once tumors reached approximately 250 mm^3, *dl*922-947 or vehicle was injected intratumorally (single injection, 1×10^{10} particles in 50 μl PBS). A single dose of i.p. UCN-01 or vehicle (7.5 mg/kg in 20% icodextrin) was administered 24 hours later. Mice were killed 24 hours thereafter. Tumors were excised and fixed in 10% formal-buffered saline (n = 2 per group) or snap frozen in dry ice (n = 3 per group). Fixed tumors were transferred to ice-cold 70% ethanol after 24 hours, and 4-μm sections were cut and processed. E1A expression was detected using a rabbit anti-Ad2 E1A antibody (Santa Cruz Biotechnology Inc.). Total RNA was extracted from snap-frozen tumors using TRIzol. After DNAse digestion (Qiagen), 1 μg total RNA was reverse transcribed using random hexonucleotide primers (First-Strand Synthesis Kit, Roche) and analyzed by quantitative PCR. For assessment of antitumor efficacy, 5×10^6 IGROV1-luciferase or A2780CP-luciferase cells were inoculated i.p. into female *nu/nu* mice on day 1. In IGROV1 experiments, *dl*922-947 or control adenovirus CMV-GFP (5×10^9 particles in 400 μl 20% icodextrin) were injected i.p. on days 9, 10, 15, and 16. UCN-01 (5 mg/kg) or vehicle (20% icodextrin) were administered i.p. on days 11, 12, 17, and 18. For A2780CP experiments, virus was administered on days 9, 11, 15, and 17, and UCN-01/vehicle were administered on days 10, 12, 16, and 18. Mice were injected i.p. with 125 mg/kg D-luciferin (Calliper Life Sciences) and then anesthetized (2% isoflurane by inhalation). Five minutes later, while still under anesthetic, they were placed in a light-tight chamber on a warmed stage (37°C), and light emission from a defined region of interest on the ventral aspect was imaged on a Xenogen IVIS Imaging System 100 (Alameda). Data were analyzed using Living Image software (also Xenogen) and are presented as mean radiance (photons/s/cm^2/steradian [photons/s/cm^2/sr]).

Statistics. All statistical analyses were generated with GraphPad Prism 5.00. All analyses are unpaired, 2-tailed Student's t-test unless otherwise stated. All experiments were performed in triplicate and error bars represent SD unless otherwise stated. P values of less than 0.05 were considered significant.

Acknowledgments

This work is supported by the Medical Research Council (grant reference G0601891). We would like to thank Mohammed Ikram for assistance with immunohistochemistry and Ingrid Hoffman (German Cancer Research Center, Heidelberg, Germany), who donated the plasmid pX-HA-Cdc25A.

Received for publication November 22, 2010, and accepted in revised form January 12, 2011.

Address correspondence to: Iain A. McNeish, Centre for Molecular Oncology and Imaging, John Vane Science Centre, Charterhouse Square, London, EC1M 6BQ, United Kingdom. Phone: 44.20.7882.3840; Fax: 44.20.7882.3884; E-mail: i.a.mcneish@qmul.ac.uk.

Sally P. Wheatley's present address is: School of Biomedical Sciences, University of Nottingham, Nottingham, United Kingdom.

1. Fattaey AR, Harlow E, Helin K. Independent regions of adenovirus E1A are required for binding to and dissociation of E2F-protein complexes. *Mol Cell Biol*. 1993;13(12):7267–7277.
2. Heise C, et al. An adenovirus E1A mutant that demonstrates potent and selective systemic anti-tumoral efficacy. *Nat Med*. 2000;6(10):1134–1139.
3. Lockley M, et al. Activity of the adenoviral E1A deletion mutant dl922-947 in ovarian cancer: comparison with adenovirus wild-type, bioluminescence monitoring and intraperitoneal delivery in icodextrin. *Cancer Res*. 2006;66(2):989–998.
4. Sherr CJ, McCormick F. The RB and p53 pathways in cancer. *Cancer Cell*. 2002;2(2):103–112.
5. D'Andrilli G, Kumar C, Scambia G, Giordano A. Cell cycle genes in ovarian cancer: steps toward earlier diagnosis and novel therapies. *Clin Cancer Res*. 2004;10(24):8132–8141.
6. Yaginuma Y, et al. Analysis of the Rb gene and cyclin-dependent kinase 4 inhibitor genes (p16INK4 and p15INK4B) in human ovarian carcinoma cell lines. *Exp Cell Res*. 1997;233(2):233–239.
7. Baird SK, Aerts JL, Eddaoudi A, Lockley M, Lemoine NR, McNeish IA. Oncolytic adenoviral mutants induce a novel mode of programmed cell death in ovarian cancer. *Oncogene*. 2008;27(22):3081–3090.
8. Flak MB, et al. p21 promotes oncolytic adenoviral activity in ovarian cancer and is a potential biomarker. *Mol Cancer*. 2010;9:175.
9. Jones N, Shenk T. An adenovirus type 5 early gene function regulates expression of other early viral genes. *Proc Natl Acad Sci U S A*. 1979;76(8):3665–3669.
10. Connell CM, Wheatley SP, McNeish IA. Nuclear survivin abrogates multiple cell cycle checkpoints and enhances viral oncolysis. *Cancer Res*. 2008; 69(19):7923–7931.
11. Saleh-Gohari N, Bryant HE, Schultz N, Parker KM, Cassel TN, Helleday T. Spontaneous homologous recombination is induced by collapsed replication forks that are caused by endogenous DNA single-strand breaks. *Mol Cell Biol*. 2005;25(16):7158–7169.
12. Cherubini G, Petouchoff T, Grossi M, Piersanti S, Cundari E, Saggio I. E1B55K-deleted adenovirus (ONYX-015) overrides G1/S and G2/M checkpoints and causes mitotic catastrophe and endoreduplication in p53-proficient normal cells. *Cell Cycle*. 2006;5(19):2244–2252.
13. Blackford AN, et al. A role for E1B-AP5 in ATR signaling pathways during adenovirus infection. *J Virol*. 2008;82(15):7640–7652.
14. Carson CT, et al. Mislocalization of the MRN complex prevents ATR signaling during adenovirus infection. *Embo J*. 2009;28(6):652–662.
15. Karen KF, Hoey PJ, Young CS, Hearing P. Temporal regulation of the Mre11-Rad50-Nbs1 complex during adenovirus infection. *J Virol*. 2009;83(9):4565–4573.
16. Nichols GJ, Schaack J, Ornelles DA. Widespread phosphorylation of histone H2AX by species C adenovirus infection requires viral DNA replication. *J Virol*. 2009;83(12):5987–5998.
17. Kimball KJ, et al. A phase I study of a tropism-modified conditionally replicative adenovirus for recurrent malignant gynecologic diseases. *Clin Cancer Res*. 2010;16(21):5277–5287.
18. Hearing P, Shenk T. The adenovirus type 5 E1A enhancer contains two functionally distinct domains: one is specific for E1A and the other modulates all early units in *cis*. *Cell*. 1986;45(2):229–236.
19. Murray JD, Braithwaite AW, Taylor IW, Bellett AJ. Adenovirus-induced alterations of the cell growth cycle: effects of mutations in early regions E2A and E2B. *J Virol*. 1982;44(3):1072–1075.
20. Braithwaite AW, Murray JD, Bellett AJ. Alterations to controls of cellular DNA synthesis by adenovirus infection. *J Virol*. 1981;39(2):331–340.
21. Machida YJ, Dutta A. Cellular checkpoint mechanisms monitoring proper initiation of DNA replication. *J Biol Chem*. 2005;280(8):6253–6256.
22. Huang X, Darzynkiewicz Z. Cytometric assessment of histone H2AX phosphorylation: a reporter of DNA damage. *Methods Mol Biol*. 2006;314:73–80.
23. Caporossi D, Bacchetti S. Definition of adenovirus type 5 functions involved in the induction of chromosomal aberrations in human cells. *J Gen Virol*. 1990;71(pt 4):801–808.
24. Ornelles DA, Shenk T. Localization of the adenovirus early region 1B 55-kilodalton protein during lytic infection: association with nuclear viral inclusions requires the early region 4 34-kilodalton protein. *J Virol*. 1991;65(1):424–429.
25. Susin SA, et al. Molecular characterization of mitochondrial apoptosis-inducing factor. *Nature*. 1999;397(6718):441–446.
26. Ward IM, Chen J. Histone H2AX is phosphorylated in an ATR-dependent manner in response to replicational stress. *J Biol Chem*. 2001;276(51):47759–47762.
27. Zhao B, et al. Structural basis for Chk1 inhibition by UCN-01. *J Biol Chem*. 2002;277(48):46609–46615.
28. Arnaudeau C, Lundin C, Helleday T. DNA double-strand breaks associated with replication forks are predominantly repaired by homologous recombination involving an exchange mechanism in mammalian cells. *J Mol Biol*. 2001;307(5):1235–1245.
29. Li X, Heyer WD. Homologous recombination in DNA repair and DNA damage tolerance. *Cell Res*. 2008;18(1):99–113.
30. Blasina A, et al. Breaching the DNA damage checkpoint via PF-00477736, a novel small-molecule inhibitor of checkpoint kinase 1. *Mol Cancer Ther*. 2008;7(8):2394–2404.
31. Spitkovsky D, Jansen-Durr P, Karsenti E, Hoffman I.

S-phase induction by adenovirus E1A requires activation of cdc25a tyrosine phosphatase. *Oncogene*. 1996;12(12):2549–2554.
32. Molinari M, Mercurio C, Dominguez J, Goubin F, Draetta GF. Human Cdc25 A inactivation in response to S phase inhibition and its role in preventing premature mitosis. *EMBO Rep*. 2000; 1(1):71–79.
33. Blomberg I, Hoffmann I. Ectopic expression of Cdc25A accelerates the G(1)/S transition and leads to premature activation of cyclin E- and cyclin A-dependent kinases. *Mol Cell Biol*. 1999;19(9):6183–6194.
34. Mailand N, et al. Rapid destruction of human Cdc25A in response to DNA damage. *Science*. 2000;288(5470):1425–1429.
35. Sorensen CS, Syljuasen RG, Lukas J, Bartek J. ATR, Claspin and the Rad9-Rad1-Hus1 complex regulate Chk1 and Cdc25A in the absence of DNA damage. *Cell Cycle*. 2004;3(7):941–945.
36. Sorensen CS, et al. The cell-cycle checkpoint kinase Chk1 is required for mammalian homologous recombination repair. *Nat Cell Biol*. 2005;7(2):195–201.
37. Harada JN, Shevchenko A, Pallas DC, Berk AJ. Analysis of the adenovirus E1B-55K-anchored proteome reveals its link to ubiquitination machinery. *J Virol*. 2002;76(18):9194–9206.
38. Bryant HE, et al. Specific killing of BRCA2-deficient tumours with inhibitors of poly(ADP-ribose) polymerase. *Nature*. 2005;434(7035):913–917.
39. Katich SC, Zerfass-Thome K, Hoffmann I. Regulation of the Cdc25A gene by the human papillomavirus Type 16 E7 oncogene. *Oncogene*. 2001; 20(5):543–550.
40. Sorensen CS, et al. Chk1 regulates the S phase checkpoint by coupling the physiological turnover and ionizing radiation-induced accelerated proteolysis of Cdc25A. *Cancer Cell*. 2003;3(3):247–258.
41. Baker A, Rohleder KJ, Hanakahi LA, Ketner G. Adenovirus E4 34k and E1b 55k oncoproteins target host DNA ligase IV for proteasomal degradation. *J Virol*. 2007;81(13):7034–7040.
42. Ingemarsdotter CK, Baird SK, Connell CM, Oberg D, Hallden G, McNeish IA. Low-dose paclitaxel synergizes with oncolytic adenoviruses via mitotic slippage and apoptosis in ovarian cancer. *Oncogene*. 2010;29(45):6051–6063.
43. Shenk T. Adenoviridae: the viruses and their replication. In: Knipe DM, Howley PM, eds. *Fields Virology*. 4th ed. Philadelphia, Pennsylvania, USA: Lippincott, Williams and Wilkins; 2001:2265–2300.
44. Howe JA, Bayley ST. Effects of Ad5 E1A mutant viruses on the cell cycle in relation to the binding of cellular proteins including the retinoblastoma protein and cyclin A. *Virology*. 1992;186(1):15–24.
45. Wang HG, Draetta G, Moran E. E1A induces phosphorylation of the retinoblastoma protein independently of direct physical association between the E1A and retinoblastoma products. *Mol Cell Biol*. 1991;11(8):4253–4265.
46. Farmer H, et al. Targeting the DNA repair defect in BRCA mutant cells as a therapeutic strategy. *Nature*. 2005;434(7035):917–921.
47. Fong PC, et al. Poly(ADP)-Ribose Polymerase Inhibition: Frequent Durable Responses in BRCA Carrier Ovarian Cancer Correlating With Platinum-Free Interval. *J Clin Oncol*. 2010;28(15):2512–2519.
48. Hotte SJ, et al. Phase I trial of UCN-01 in combination with topotecan in patients with advanced solid cancers: a Princess Margaret Hospital Phase II Consortium study. *Ann Oncol*. 2006;17(2):334–340.
49. McNeish IA, Tenev T, Bell S, Marani M, Vassaux G, Lemoine N. Herpes simplex virus thymidine kinase/ganciclovir-induced cell death is enhanced by co-expression of caspase-3 in ovarian carcinoma cells. *Cancer Gene Ther*. 2001;8(4):308–319.